Contrib Mineral Petrol (2006) 152:571–589
DOI 10.1007/s00410-006-0119-y

ORIGINAL PAPER

Nd, Pb, and Sr isotope composition of juvenile magmatism in the Mesozoic large magmatic province of northern Chile (18–27°S): indications for a uniform subarc mantle

Friedrich Lucassen · Wolfgang Kramer · Viola Bartsch · Hans-Gerhard Wilke · Gerhard Franz · Rolf L. Romer · Peter Dulski

Received: 20 January 2006 / Accepted: 12 June 2006 / Published online: 1 August 2006
© Springer-Verlag 2006

Abstract The Jurassic to Early Cretaceous magmatic arc of the Andes in northern Chile was a site of major additions of juvenile magmas from the subarc mantle to the continental crust. The combined effect of extension and a near stationary position of the Jurassic to lower Cretaceous arc favoured the emplacement and preservation of juvenile magmatic rocks on a large vertical and horizontal scale. Chemical and Sr, Nd, and Pb isotopic compositions of mainly mafic to intermediate volcanic and intrusive rock units coherently indicate the generation of the magmas in a subduction regime and the dominance of a depleted subarc mantle source over contributions of the ambient Palaeozoic crust. The isotopic composition of the Jurassic ($^{206}Pb/^{204}Pb$: ~ 18.2; $^{207}Pb/^{204}Pb$: ~ 15.55; $^{143}Nd/^{144}Nd$: ~ 0.51277; $^{87}Sr/^{86}Sr$: ~ 0.703–0.704) and Present ($^{206}Pb/^{204}Pb$: ~ 18.5; $^{207}Pb/^{204}Pb$: ~ 15.57; 143Nd/144Nd: ~ 0.51288; $^{87}Sr/^{86}Sr$: ~ 0.703–0.704) depleted subarc mantle beneath the Central and Southern Andes (18°–40°S) was likely uniform over the entire region. Small differences of isotope ratios between Jurassic and Cenozoic to Recent of subarc mantle-derived could be explained by radiogenic growth in a still uniform mantle source.

Communicated by J. Hoefs

Electronic Supplementary Material Supplementary material is available to authorised users in the online version of this article at http://dx.doi.org/10.1007/s00410-006-0119-y.

F. Lucassen (✉) · W. Kramer · R. L. Romer · P. Dulski
GeoForschungsZentrum Potsdam, Telegrafenberg,
14473 Potsdam, Germany
e-mail: lucassen@gfz-potsdam.de

V. Bartsch · G. Franz
Fachgebiet Petrologie—BH 1, Technische Universität
Berlin, Strasse des 17.Juni 135, 10623 Berlin, Germany

H.-G. Wilke
Departamento Ciencias Geológicas, Universidad Católica
del Norte, Antofagasta, Casilla 1280, Chile

Introduction

Magmatic arcs are a principal site of extraction of new crustal material from the asthenospheric mantle (e.g. Ernst 2000). This material is either accreted to the continents by the collision of oceanic island arcs or incorporated directly into the crust of continental magmatic arcs. The Mesozoic to Recent western margin of the South American continent in the Central Andes (18°–27°S) is an example of a continental magmatic arc without accretion of allochthonous material (e.g. Scheuber et al. 1994). The Jurassic to Early Cretaceous is an exceptional period in the Phanerozoic evolution of this continental margin, because large volumes of mafic to intermediate juvenile rocks formed and are preserved (Fig. 1a). The estimated volume of the juvenile plutonic and volcanic rocks at 18–27°S is 1.25–2.5 × 10^6 km^3 (see our estimation below) and comparable to the volume of some large igneous provinces (LIP; e.g. Coffin and Eldholm 1994). The depositional features, volume, and composition of the volcanic units in the Jurassic arc are very different from those of the Cenozoic Andean volcanism. Lava flows from fissure eruptions are common and form several kilometer thick piles of volcanic rocks (e.g. Palacios 1978; Buchelt and Tellez 1988; Vergara et al. 1995; Németh et al. 2004; Kramer et al. 2005) and are widely distributed in basin like structures

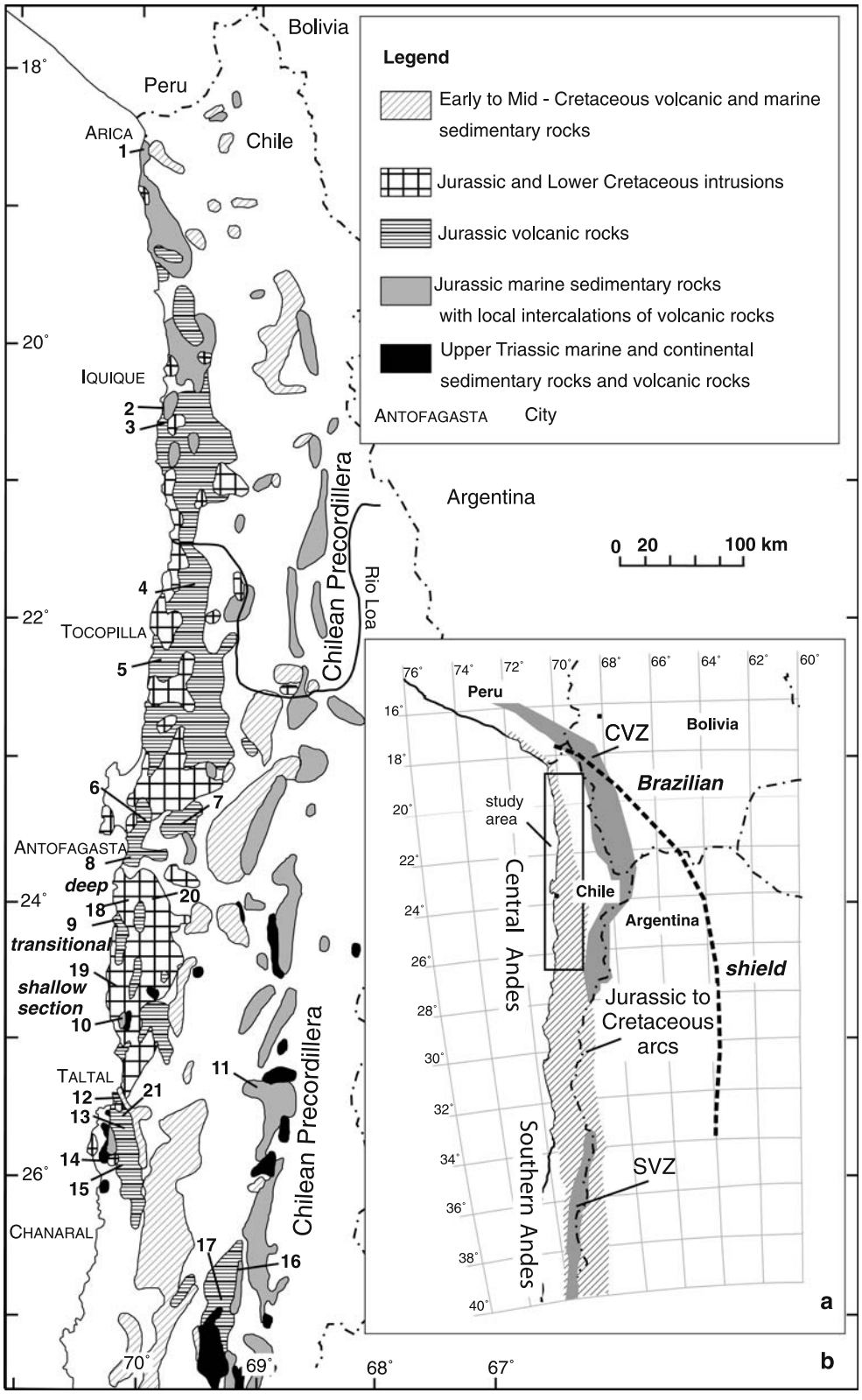

rather than strato volcanoes and relatively thin cover of volcanic rocks as it is typical of volcanic rocks in the Cenozoic magmatic arc (e.g. Francis and Hawkesworth 1994).

The purpose of the paper is (1) to characterize the Sr-, Nd- and Pb isotopic composition of the subarc mantle source in the Early Mesozoic magmatic arc of northern Chile on the basis of our new data on plutonic

◄ **Fig. 1** **a** Jurassic to lower Cretaceous magmatic arc of northern and central Chile (*hatched area*) and its continuation into the Cretaceous to Tertiary arc of southern central Chile and the presently active arc (*CVZ* Central Volcanic zone, *SVZ* Southern Volcanic Zone). The late Carboniferous to Permo - Triassic arc extends from the Costal Cordillera of northern and central Chile into Precordillera of northern Chile (west of the CVZ) and into the principal Cordillera (the location of the SVZ) of southern central Chile. The map is redrawn and modified from Schobbenhaus and Bellizzia (2001). The *stippled line* indicates the tentatively drawn border between the crust reworked during Early Palaeozoic in the west and the Proterozoic Brazilian shield (Lucassen et al. 2000). **b** Major surface occurrences of Triassic, Jurassic, and lower to mid Cretaceous igneous rocks and sedimentary rocks with volcanic intercalations, the approximate position of the deep, transitional, and shallow sections of the Coastal batholith between Antofagasta and Taltal and sample locations (see Table A1). Map redrawn from Hoja Geologica 1:1,000,000 (Servicio Nacional De Geología y Minería 1982, Santiago, Chile) and Reutter et al. (1994). Key to the sample locations: *Volcanic rocks*: *1* Coast, S of Arica*; *2* Coast, S of Iquique*; *3* Oficina Viz, Pampa de la Union*; *4* Cerro Quillagua; *5* Punta Alala; *6* Sierra Miranda, NNE of Antofagasta; *7* Cerro Mantos Blancos, NE of Antofagasta; *8* Quebrada La Negra, S of Antofagasta; *9* Caleta Agua Salada**; *10* Cerro Yumbes (Triassic); *11* Sierra de Candeleros; *12* S of Taltal, Cerro Blanco, Cerro Plomo; *13* Cerro del Difunto; *14* Quebrada Cachina (Triassic); *15* Sierra Minillas; *16* Quebrada la Tranquita; *17* Sierra Fraga; *plutonic rocks*: *18* deep section of the Coastal batholith**; *19* shallow section of the Coastal batholith; 20 Cerro Cristales; late Jurassic and early Cretaceous *dikes*: 18 deep section of the Coastal batholith**; 21 Cerro Argolla, S. of Taltal. Additional sample locations: *(Kramer et al. 2005), **(Lucassen et al. 2002)

and volcanic rocks and to trace the evolution of the subarc mantle source in the isotopic compositions of mainly Cenozoic to Quaternary magmatic rocks of the Central and southern Andes (Fig. 1). (2) We evaluate, how the composition of this Early Mesozoic magmatism and its tectonic setting relates to other near contemporaneous or younger sections of the same active continental margin in central Chile and Peru.

The situation in continental magmatic arcs is complex and compositional effects of material transfer into the mantle wedge could comprise additions from altered oceanic crust, subducted oceanic and continental sediments, continental crust from subduction erosion of the forearc, and older lithospheric mantle the latter especially during periods of lithospheric shortening as in the Cenozoic Andes. A reasonable resolution of these different additions to the subarc mantle seems impossible in fossil arcs, if no characteristic signatures are related. Our approach is to consider the subarc mantle as it is including the possible additions to the mantle wedge and to distinguish hybridization processes within the crust on a large regional and time scale using the common radiogenic isotope signatures.

Geological setting

This study focuses on the area of the Coastal Cordillera in northern Chile at 18–27°S (Fig. 1) where a continental magmatic arc was active from Latest Triassic to Early Cretaceous (Fig. 1b). Conclusions drawn from this work are applicable to similar situations south and north of our study area in the Coastal to Principal Cordillera of the southern Andes at 28–40°S (e.g. Vergara et al. 1995; Morata and Aguirre 2003; Lucassen et al. 2004) and the Coast range of southern and central Peru (e.g. contributions in Pitcher et al. 1985; Romeuf et al. 1993). Most of the exposed igneous rocks in the whole area are volcanic, but the study area is unique insofar as it includes a more eroded, deformed, and partly metamorphosed section of a composite batholith at ca. 24°S. The erosion level becomes shallower towards the south (ca. 26°S; Fig. 1b) and therefore allows studying the deep plutonic, the subvolcanic, and the volcanic section in close spatial relationship.

Mesozoic volcanic rocks of the coastal area of Copiapo and Iquique, northern Chile, have already been described by Ch. Darwin as the 'porphyritic conglomerate formation' (Darwin, Ch., Geological observations on South America, available as Project Gutenberg Etext South American Geology, by Charles Darwin http://www.gutenberg.org/etext/3620). Since then, the area has been place of numerous detailed studies and surveys of the Jurassic magmatism and its tectonic setting and the Mesozoic sedimentary evolution. The structure of the deeper crust is known from geophysical studies, which show a large, north–south extended prominent positive gravity anomaly along the Coastal Cordillera of northern Chile (Götze and Kirchner 1997) and higher seismic velocities in the crust of the Jurassic-Cretaceous magmatic arc than in the Early Palaeozoic crust east of the arc (ca. 24°–21°S; e.g. Wigger et al. 1994; Oncken et al. 2003). The high densities and seismic velocities require substantial volumes of mafic to intermediate rocks in the crust of the arc and indicate that the surface expression with the large amount of mafic rocks continues to depth.

The pre-Mesozoic basement

The western continental margin of South America was periodically active at least from the Early Palaeozoic onwards (e.g. Coira et al. 1982), and the geological processes at this site formed the basement for the Jurassic magmatic arc. The basement is considered as a Palaeozoic mobile belt at the western edge of Gondwana. It consists of reworked crustal material with a peak of the Nd isotope model ages of its

metamorphic and felsic magmatic rocks at 1.8–2.0 Ga; inherited ages from zircons centre at ca. 1.1 and 2.0 Ga (e.g. Lucassen et al. 2001 and references therein). These ages mirror the age structure of the western part of the South American craton, where important crustal growth occurred at ca. 2 Ga and a metamorphic-magmatic cycle at ca. 1.1 Ga (Cordani et al. 2000; Sato and Siga 2002).

The Palaeozoic crust is likely to be of mainly felsic composition, because magmatism (e.g. Lucassen et al. 2001) and sedimentation (Bock et al. 2000) throughout the Palaeozoic was dominated by rocks containing high proportions of recycled Proterozoic continental crust, whereas juvenile mantle-derived magmatic rocks are scarce. The oldest rocks of the sampling area are mainly felsic Early Palaeozoic metamorphic rocks, which occur in small, scattered outcrops (Damm et al. 1994; Lucassen et al. 1999, 2000, 2001). Early Palaeozoic ages of high T and moderate P metamorphic conditions correspond with the ages and P–T conditions of extended occurrences of metamorphic and magmatic rocks in western Argentina (e.g. Pankhurst and Rapela 1998; Lucassen and Becchio 2003). We consider the Palaeozoic crust as the principal component (1) in the generation of crustal melts, (2) for assimilation by mantle derived melts in the crust and (iii) for the input from the continent into the Jurassic subduction zone either through sediment-subduction or tectonic erosion from the upper plate.

The Jurassic arc (18–27°S)

The Latest Triassic is transitional to the Jurassic regime. A marine ingression occurred in the Latest Triassic (Tankard et al. 1995) into extensional basins and bimodal volcanism is related to these structures (e.g. Suarez and Bell 1992; Morata et al. 2000). In the working area, small-volume Triassic silicic to intermediate volcanic rocks are intercalated with Latest Triassic continental to shallow marine sedimentary rocks (Gröschke et al. 1988; Suarez and Bell 1992; Bebiolka 1999; Bartsch 2004; Fig. 1b: sample locations of Latest Triassic volcanic rocks). Scarce Triassic intrusions (Berg and Baumann 1985) in the working area were not investigated in the course of this study.

The dominant depositional features of the Jurassic up to the Early Cretaceous volcanic rocks are sheet like extrusions from fissures with abundant lava flows. Single volcanic edifices are rare. Extrusion was during the whole activity close to sea level and sub-aquatic deposition of lava flows occurred repeatedly (for details see: Kossler 1998; Bartsch 2004; Németh et al. 2004; Kramer et al. 2005). The deposition of the thick volcanic sequence in subsiding structures is linked to dominantly extensional tectonics (e.g. Pichowiak 1994; Scheuber and Gonzales 1999; Grocott and Taylor 2002). The sedimentation in the adjacent shallow marine basins in the back-arc region was largely undisturbed by tectonic movements and occurred in generally slowly subsiding basins with periodically active depocentres (Prinz et al. 1994; Ardill et al. 1998).

The Jurassic volcanism started on a large regional scale at around 200 Ma. Precise timing of the Jurassic volcanism by isotopic dating remains problematic, because many volcanic rocks show a hydrothermal overprint by seawater-rock interaction or by abundant later intrusions. Burial metamorphism is likely, as known from other thick piles of mainly Early Cretaceous volcanic rocks from an identical setting in central Chile (e.g. Levi et al. 1989; Aguirre et al. 1999). The local intercalation of volcanic and shallow marine sedimentary rocks enables biostratigraphic age bracketing in various sections of the arc (ages in Table 1 and Table A1). Between Taltal and Tocopilla the onset of the Jurassic volcanism was in the Sinemurian (200–191 Ma; stratigraphic ages from International Stratigraphic Chart IUGS, 2000, ISBN 0–930423–22-4), whereas north of Tocopilla the onset was in the Bajocian (170–164 Ma) according to biostratigraphic markers (Gröschke et al. 1988; Prinz et al. 1994; Kossler 1998; Hillebrandt et al. 2000; Wittmann 2001). Earliest spatially related intrusions occur around 200–185 Ma (Berg and Baumann 1985; Rogers and Hawkesworth 1989; Pichowiak 1994; Dallmeyer et al. 1996; Lucassen and Thirlwall 1998). Biostratigraphic constraints allow a tentative subdivision of the volcanic rocks until the Bajocian (Bartsch 2004) and, north of Tocopilla, until the Oxfordian (154–146 Ma; Kramer et al. 2005), where the Jurassic volcanic rocks are unconformably overlain by Early Cretaceous volcano-sedimentary rocks (Hillebrandt et al. 2000; Wittmann 2001). In the Early Cretaceous, the main activity of the arc shifted towards the east, partly overlapping with the Jurassic arc especially in the southern section (Fig. 1b). The sample set of the volcanic rocks comprises various profiles from the southern (Bartsch 2004; Lucassen et al. 2002) and northern part (Kramer et al. 2005) supplemented by profiles from the Tocopilla and Antofagasta area (Fig. 1b).

The Coastal batholith in the study area is subdivided into a deep, transitional, and shallow section. The deep section of the Coastal batholith is exposed south of Antofagasta (23°45′–24°S; Fig. 1b; Rössling 1989; Lucassen and Franz 1996; Gonzales 1996; Scheuber and Gonzales 1999) and comprises mafic to intermediate (meta) plutonic rocks with uniform mineralogy

Table 1 Newly acquired Sr, Nd and Pb isotope data and sample locations (Fig. 1b)

Sample	Age (Ma)	Rb (ppm)	Sr (ppm)	$^{87}Rb/^{86}Sr'$	$^{87}Sr/^{86}Sr \pm 2\sigma m$	$^{87}Sr/^{86}Sr$ initial	Sm (ppm)	Nd (ppm)	$^{147}Sm/^{144}Nd$	$^{143}Nd/^{144}Nd \pm 2\sigma$ m	$^{143}Nd\epsilon^{144}Nd$ initial	ϵ-Nd initial
Jurassic volcanic rocks												
	Cerro Quillagua (5); 21°40′00″, 69°49′30″											
262	*195*	32	440	**0.210**	0.704157 ± 10	0.70358	1.50	6.80	0.133	0.512843 ± 5	0.51267	5.6
	Punta Alala (5); 22°16′00″, 70°17′10''											
266	*186*	4	123	**0.096**	0.705382 ± 8	0.70513	3.70	14.0	0.160	0.512830 ± 9	0.51264	4.6
	Quebrada La Negra (8); 23°24′30″, 70°22′00″											
164	*186*	21	347	**0.174**	0.703439 ± 10	0.70298	3.40	13.00	0.158	0.512946 ± 5	0.51275	6.9
	Sierra de Candeleros (11) 25°20′, 69°25′''											
K 51[a]	*163*	32	531	**0.174**	0.705018 ± 10	0.70462	8.90	35.00	0.154	0.512847 ± 5	0.51268	5.0
	S. of Taltal (12), Cerro Blanco (samples 1,2; 25°24′30″, 70°30′40″), Cerro Plomo (25°27′45″, '70°31′13″)											
96–310[a]	*170*	91	393	0.667	0.706257 ± 10	0.70464	5.30	20.00	0.160	0.512997 ± 5	0.51282	7.8
	Cerro del Difunto (13); 25°41′30″, 70°32′50″											
96–21[a]	*194*	21	210	**0.288**	0.705092 ± 10	0.70430	3.60	12.20	0.178	0.512800 ± 5	0.51257	3.6
95–21[a]	*154*	75	256	0.844	0.705717 ± 10	0.70387	6.30	26.00	0.147	0.512777 ± 5	0.51263	3.7
95–45[a]	*154*	147	398	1.065	0.708300 ± 10	0.70597	4.30	16.00	0.163	0.512856 ± 5	0.51269	4.9
95–70 a[a]	*154*	48	252	0.549	0.704974 ± 10	0.70377	5.70	22.00	0.157	0.512800 ± 5	0.51264	3.9
96–192[a]	*140*	34	439	**0.223**	0.704147 ± 10	0.70370	2.80	11.00	0.154	0.512885 ± 5	0.51274	5.6
9	160	35	74	1.376	0.708201 ± 10	0.70507	5.92	23.46	0.153	0.512857 ± 5	0.51270	5.2
	Quebrada la Tranquita (16); 26°39′40″, 69°32′10″											
K 32[a]	*165*	18	353	**0.147**	0.704087 ± 10	0.70375	6.60	26.0	0.154	0.512850 ± 5	0.51269	5.0
	Sierra Fraga (17); 27°00′, 69°48′											
97–5	*160*	44	261	0.486	0.704578 ± 11	0.70347	6.60	25.0	0.160	0.512953 ± 5	0.51279	7.1
Triassic volcanic rocks												
	Cerro Yumbes (10); 24°55′33″, 70°27′51″											
97–213	*211*	10	48	0.581	0.708705 ± 9	0.70696	1.67	7.24	0.139	0.512412 ± 4	0.51222	–2.9
97–218	*211*	122	98	3.610	0.718541 ± 9	0.70771	7.05	35.0	0.122	0.512390 ± 5	0.51222	–2.8
	Quebrada Cachina (14); 25°52′30″, 70°35′40″											
96–77a[a]	211	28	212	0.381	0.705853 ± 10	0.70471	2.90	14.0	0.125	0.512631 ± 5	0.51246	1.8
K 116	211	149	90	4.773	0.718847 ± 7	0.70453	4.34	22.6	0.116	0.512597 ± 5	0.51244	1.4
K 118	211	122	142	2.477	0.711035 ± 10	0.70360	4.35	19.4	0.135	0.512721 ± 8	0.51253	3.3
Early Cretaceous dikes												
	Cerro Argolla, S. of Taltal (21); 25°28′, 70°30″											
115	140	114	227	1.448	0.707487 ± 8	0.70461	10.3	44.6	0.140	0.512723 ± 5	0.51260	2.7
181	140	61	196	0.900	0.705423 ± 8	0.70363	11.4	44.7	0.154	0.512905 ± 5	0.51276	6.0
203	140	143	214	1.927	0.708806 ± 11	0.70497	10.2	44.7	0.138	0.512727 ± 6	0.51260	2.8
231	140	78	240	0.934	0.706224 ± 8	0.70436	8.10	35.1	0.140	0.512767 ± 5	0.51264	3.5
233	140	37	312	0.337	0.704350 ± 8	0.70368	8.86	35.8	0.150	0.512853 ± 5	0.51272	5.0
234	140	84	230	1.054	0.706505 ± 14	0.70441	8.94	38.1	0.142	0.512725 ± 5	0.51260	2.7
Plutonic rocks												
	Deep section of the Coastal Batholith, Cerro Cristales (20); 23°50′, 70°25′''											
U-8	140	27	428	0.181	0.703774 ± 8	0.70341	3.41	14.1	0.146	0.512876 ± 6	0.51274	5.5
U-24	140	22	411	0.156	0.703613 ± 10	0.70330	2.53	11.3	0.136	0.512858 ± 6	0.51273	5.4

Table 1 continued

Sample	Age (Ma)	Rb (ppm)	Sr (ppm)	$^{87}Rb/^{86}Sr'$	$^{87}Sr/^{86}Sr \pm 2\sigma m$	$^{87}Sr/^{86}Sr$ initial	Sm (ppm)	Nd (ppm)	$^{147}Sm/^{144}Nd$	$^{143}Nd/^{144}Nd \pm 2\sigma$ m	$^{143}Nd\epsilon^{144}Nd$ initial	ϵ-Nd initial
U-83	140	28	368	0.217	0.703728 ± 8	0.70330	2.51	11.5	0.132	0.512870 ± 5	0.51275	5.7
U-85	140	34	364	0.268	0.703857 ± 8	0.70332	3.50	15.6	0.136	0.512854 ± 7	0.51273	5.3
	Shallow section of the Coastal batholith (19) 24°58′ – 25°22′, 70°23											
MCP-1	160	81	349	0.671	0.705097 ± 10	0.70357	7.11	30.1	0.143	0.512896 ± 5	0.51275	6.1
MCP-11	160	46	224	0.585	0.705142 ± 10	0.70381	5.94	23.9	0.150	0.512886 ± 4	0.51273	5.8
QPA-2	160	4	381	0.032	0.703987 ± 11	0.70391	3.87	17.0	0.138	0.512887 ± 5	0.51274	6.1
QPA-4	160	53	342	0.445	0.704419 ± 8	0.70341	6.15	26.2	0.142	0.512882 ± 5	0.51273	5.9
QMA-1	160	118	356	0.955	0.705530 ± 11	0.70336	5.43	24.9	0.132	0.512803 ± 3	0.51266	4.5
QMA-2	160	164	219	2.159	0.708028 ± 10	0.70312	5.95	27.1	0.133	0.512815 ± 5	0.51268	4.8
QBA-1	160	152	243	1.803	0.707612 ± 16	0.70351	5.91	25.9	0.138	0.512784 ± 4	0.51264	4.0
QBA-5	160	95	222	1.232	0.706692 ± 10	0.70389	4.33	22.8	0.115	0.512808 ± 4	0.51269	5.0
QSR-1	160	48	385	0.362	0.704395 ± 11	0.70357	3.71	17.2	0.130	0.512740 ± 6	0.51260	3.3
QSR-8	160	17	630	0.078	0.704067 ± 8	0.70389	1.88	6.31	0.180	0.512859 ± 5	0.51267	4.7
QCA-5	160	39	250	0.447	0.707256 ± 8	0.70624	6.28	30.5	0.125	0.512585 ± 5	0.51245	0.4
QCA-6	160	34	322	0.307	0.706186 ± 13	0.70549	6.53	32.5	0.121	0.512628 ± 7	0.51250	1.3
QCA-7	160	133	228	1.682	0.708603 ± 13	0.70478	4.7	18.3	0.155	0.512676 ± 5	0.51251	1.6
QCA-9	160	56	387	0.417	0.704446 ± 8	0.70350	3.64	17.3	0.128	0.512688 ± 5	0.51255	2.4
QCA-1	160	155	59	7.596	0.730523 ± 9	0.71324	6.85	34.2	0.121	0.512127 ± 8	0.51200	–8.4
QCA-2	160	143	54	7.662	0.730414 ± 9	0.71299	7.05	36.2	0.118	0.512119 ± 8	0.51200	–8.5
QCA-3	160	47	61	2.240	0.715595 ± 9	0.71050	2.36	10.4	0.138	0.512143 ± 5	0.51200	–8.5
MCP-5	160	0.7	17	0.118	0.704683 ± 8	0.70441	2.53	13.2	0.116	0.512855 ± 6	0.51273	5.9

Sample	Pb (ppm)	U (ppm)	Th (ppm)	μ	ϖ	$^{206}Pb/^{204}Pb$	Initial	$^{207}Pb/^{204}Pb$	Initial	$^{208}Pb/^{204}Pb$	Initial
Jurassic volcanic rocks											
	Cerro Quillagua (5); 21°40′00″, 69°49′30″										
262	2.8	0.14	0.4	**4**	10	18.45	18.34	15.59	15.59	38.29	38.19
	Punta Alala (5); 22°16′00″, 70°17′10''										
266	4.1	0.50	1.8	**9**	32	18.49	18.23	15.59	15.58	38.36	38.06
	Quebrada La Negra (8); 23°24′30″, 70°22′00″										
164	4.6	0.60	2.0	**9**	32	18.47	18.19	15.57	15.55	38.25	37.95
	Sierra de Candeleros (11) 25°20′, 69°25'''										
K 51[a]	3.9	2.1	7.9	40	151	18.91	17.89	15.60	15.55	38.80	37.58
	S. of Taltal (12), Cerro Blanco (samples 1,2; 25°24′30″, 70°30′40″), Cerro Plomo (25°27′45″, '70°31′13″)										
96–310[a]	8.2	0.41	1.5	**4**	13	18.52	18.42	15.62	15.61	38.46	38.35
	Cerro del Difunto (13); 25°41′30″, 70°32′50″										
96–21[a]	4.4	0.50	1.5	**8**	25	18.55	18.29	15.60	15.59	38.40	38.16
95–21[a]	14.0	1.2	4.7	**6**	25	18.23	18.08	15.61	15.60	38.31	38.12
95–45[a]	21.0	0.77	2.7	**3**	9	18.46	18.39	15.63	15.62	38.45	38.38
95–70 a[a]	21.0	0.83	3.6	**3**	13	18.42	18.35	15.60	15.60	38.30	38.20
96–192[a]	4.0	0.41	1.5	**8**	28	18.41	18.24	15.59	15.59	38.24	38.05
9	16.3	1.0	3.5	**4**	16	18.68	18.57	15.64	15.63	38.67	38.54

Table 1 continued

Sample	Pb (ppm)	U (ppm)	Th (ppm)	μ	ϖ	$^{206}Pb/^{204}Pb$	Initial	$^{207}Pb/^{204}Pb$	Initial	$^{208}Pb/^{204}Pb$	Initial
	Quebrada la Tranquita (16); 26°39′40″, 69°32′10″										
K 32[a]	3.4	0.86	2.6	18	56	18.61	18.15	15.58	15.56	38.37	37.92
	Sierra Fraga (17); 27°00′, 69°48′										
97–5	9.0	0.80	2.6	**7**	21	18.59	18.43	15.62	15.61	38.50	38.33
Triassic volcanic rocks											
	Cerro Yumbes (10); 24°55′33″, 70°27′51″										
97–213	0.79	2.2	16.9	269	2118	29.30	20.35	16.16	15.71	52.75	30.53
97–218	6.3	2.5	16.4	29	193	19.09	18.12	15.67	15.62	39.24	37.21
	Quebrada Cachina (14); 25°52′30″, 70°35′40″										
96–77a[a]	4.2	1.3	4.6	23	82	19.01	18.24	15.64	15.60	38.96	38.11
K 116	2.6	1.2	4.4	36	129	19.51	18.33	15.68	15.62	39.86	38.50
K 118	3.1	0.84	3.4	20	83	19.08	18.40	15.68	15.64	39.24	38.37
Early Cretaceous dikes											
	Cerro Argolla, S. of Taltal (21); 25°28′, 70°30″										
115	35.9	3.2	13.5	7	28	18.65	18.50	15.62	15.62	38.61	38.41
181	5.4	1.4	5.0	18	68	18.74	18.34	15.62	15.60	38.62	38.14
203	9.2	3.2	13.8	26	113	19.31	18.73	15.66	15.63	39.34	38.55
231	6.0	2.5	10.2	31	128	19.08	18.39	15.63	15.60	39.08	38.19
233	140	1.7	6.1	20	76	19.09	18.64	15.65	15.63	39.13	38.61
234	6.4	2.9	11.9	34	140	19.24	18.50	15.65	15.62	39.30	38.33
Plutonic rocks											
	Deep section of the Coastal Batholith, Cerro Cristales (20); 23°50′, 70°25”										
U-8	6.4	0.65	1.9	8	22	18.80	18.63	15.61	15.60	39.67	39.51
U-24	4.9	0.41	1.5	6	22	18.43	18.29	15.58	15.57	38.24	38.09
U-83	5.1	0.58	2.4	8	35	18.50	18.33	15.61	15.60	38.34	38.10
U-85	6.3	0.84	3.4	10	40	18.51	18.29	15.57	15.56	38.32	38.04
	Shallow section of the Coastal batholith (19) 24°58′ – 25°22′, 70°23										
MCP-1	5.5	3.4	12.5	47	172	19.62	18.43	15.65	15.59	39.41	38.04
MCP-11	4.2	2.9	15.3	54	290	21.41	20.05	15.74	15.67	42.12	39.82
QPA-2	2.8	1.5	9.8	40	270	20.16	19.14	15.68	15.63	40.67	38.52
QPA-4	5.7	2.0	11.5	25	151	19.18	18.54	15.63	15.59	39.03	37.83
QMA-1	11.2	5.2	26.3	35	175	19.24	18.38	15.63	15.59	38.56	37.17
QMA-2	14.1	4.1	15.4	21	81	18.74	18.20	15.62	15.59	38.70	38.06
QBA-1	18.2	3.2	14.7	13	60	18.91	18.59	15.63	15.61	38.77	38.30
QBA-5	2.7	1.3	4.7	34	128	19.01	18.15	15.63	15.59	38.99	37.97
QSR-1	4.4	0.61	3.3	10	55	18.68	18.43	15.61	15.60	38.58	38.14
QSR-8	8.9	0.26	2.5	2	20	18.53	18.48	15.61	15.61	38.54	38.38
QCA-5	5.9	2.3	14.2	29	181	19.21	18.49	15.67	15.63	39.54	38.10
QCA-6	11.5	4.0	18.6	26	121	19.01	18.36	15.65	15.61	38.96	38.00
QCA-7	30.5	2.1	10.7	5	26	18.67	18.54	15.64	15.64	38.60	38.39
QCA-9	13.2	0.92	4.5	5	25	18.60	18.47	15.63	15.63	38.58	38.39
QCA-1	15.9	1.7	11.6	8	54	18.78	18.58	15.65	15.64	38.92	38.48
QCA-2	11.1	1.7	12.6	11	85	18.88	18.59	15.65	15.63	39.12	38.45
QCA-3	20.6	1.0	5.6	4	20	18.64	18.56	15.64	15.64	38.62	38.46

Table 1 continued

Sample	Pb (ppm)	U (ppm)	Th (ppm)	μ	ϖ	$^{206}Pb/^{204}Pb$	Initial	$^{207}Pb/^{204}Pb$	Initial	$^{208}Pb/^{204}Pb$	Initial
MCP-5	0.81	0.27	2.0	25	182	18.80	18.16	15.61	15.58	39.67	38.22

The Jurassic volcanic rocks are selected from a bigger data set and $^{87}Rb/^{86}Sr$ and μ in bold letters indicate samples used in the respective isotope diagrams. The complete data set with XRF and ICP-MS data and isotope composition of the altered samples is in Table A1 of the Appendix. The sample order is N-S following the locations in Fig. 1b. 2σ uncertainties of Pb isotope ratios are better than 0.1%, as established from the replicate analyses of NBS 981 standard. Ages in italics are stratigraphic ages inferred from field relation (detailed profiles in Bartsch 2004; Kramer at al. 2005). If age bracketing from stratigraphic record or isotopic dating is unavailable, the age is arbitrarily set to 160 Ma (or 140 Ma for the latest Jurassic to early Cretaceous dikes). Ages of the plutonic rocks are inferred from available isotopic age data; for a discussion see the text

[a]Data from the Ph.D. thesis by Bartsch (2004).

and compositionally layered gabbro intrusions. These rocks were partly deformed and metamorphosed at low-pressure of ca. 0.3–0.5 GPa and temperature decreasing from granulite, amphibolite to greenschist facies conditions. The mafic unit was intruded by a uniformly composed, large quartz–diorite pluton towards the South-East (sample location 20 'Cerro Cristales' in Fig. 1b; Gonzales 1996). In general, the intrusion-level becomes shallower towards south with more quartz dioritic to granitoid compositions, but gabbroic rocks are still present in the transitional sec-

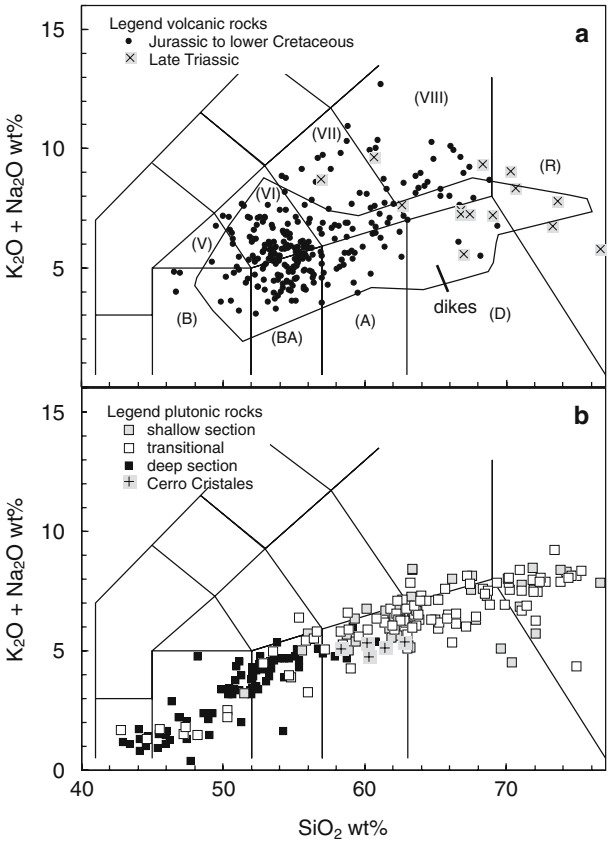

Fig. 2 Total alkali versus SiO_2 classification diagram (volatile free 100%). **a** A summary of the composition of Triassic and Jurassic to lower Cretaceous volcanic rocks from different sections of the arc; most samples plot within the fields of basaltic andesite to basaltic trachyandesite. Many rocks have subalkaline compositions typical of arc—related igneous rocks, but there are also abundant 'alkaline' compositions. (additional data: Palacios 1978; Pichowiak and Breitkreuz 1984; Buchelt and Zeil 1986; Lucassen and Franz 1994; Bartsch 2004; Kramer et al. 2005). The compositional field of the early Cretaceous dikes is similar to the one of the volcanic rocks. **b** Composition of the deep (including the Cerro Cristales pluton), transitional, and shallow section of the Coastal batholith; the *grid* is shown for easier comparison with a. (additional data: deep section, Lucassen and Franz 1994; transitional section, Marinovic et al. 1995). Key to the compositional fields: *B* basalt, *BA* basaltic andesite, *A* andesite, *D* dacite, *R* rhyolite, *V* trachy-basalt, *VI* basaltic trachy-andesite, *VII* trachy-andesite, *VIII* trachyte, Le Maitre (1989)

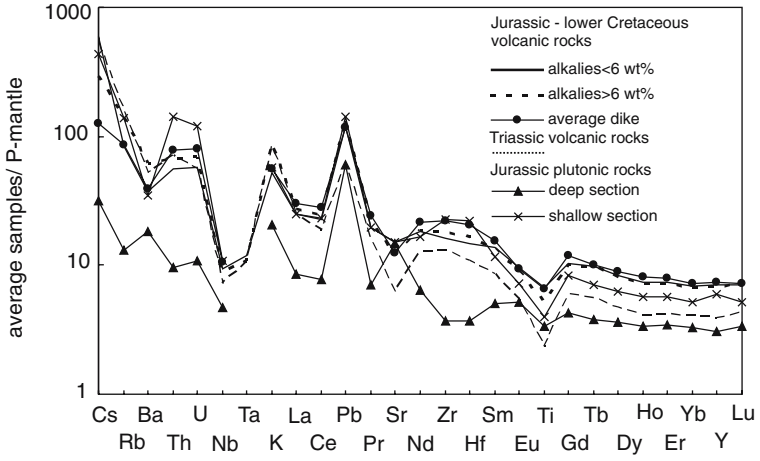

Fig. 3 Trace element patterns of average volcanic and plutonic rocks are normalized to primitive mantle (McDonough and Sun 1995). The volcanic rocks are subdivided into Triassic volcanic rocks, an alkaline and a subalkaline group of mainly Jurassic age, and late Cretaceous dikes. The differences between the four groups of volcanic and subvolcanic rocks are minor and they have element patterns typical of arc generated magmatic rocks. The plutonic rocks of the deep section comprise ultramafic cumulate rocks with more variable pattern than the more evolved rocks, but the overall patterns of the deep and shallow section of the batholith constrain their generation in the magmatic arc

tion (Marinovic and Hervé 1988; Hervé and Marinovic 1989). Pervasive deformation and metamorphism are absent in the transitional section. North of Taltal a shallow section of the batholith intrudes the Palaeozoic sedimentary cover and older units of the Jurassic volcanic rocks. Locally contacts between sedimentary rocks and the dioritic batholith are migmatite (Clarke 1998; sample location 19 Fig. 1b).

The isotopic dating of intrusions faces similar problems as that of the volcanic rocks in the deep sections of the batholith, where longstanding or repeated high temperatures were common (Lucassen and Franz 1996; Lucassen et al. 1996; Lucassen and Thirlwall 1998; Scheuber and Gonzales 1999). The age spectrum of this deep section is ca. 200–150 Ma, but the quartz diorite from the same area is ca. 140 Ma and distinctly younger than the mafic rocks (Pichowiak 1994; Lucassen and Thirlwall 1998 and references therein). K–Ar ages from the transitional section indicate a continuous magmatic activity between ca. 180 and 130 Ma (Marinovic and Hervé 1988; Hervé and Marinovic 1989; Maksaev 1990). The age of the shallow section of the Coastal batholith studied in this work is only constraint by a single age of ca. 160 Ma (K–Ar on biotite; Naranjo and Puig 1984), but this age coincides with the 160 Ma age group distinguished in a shallow section of the Coastal batholith further to the south (ca. 26°–27°S; e.g. Dallmeyer et al. 1996; Wilson et al. 2000). The other age groups from this area are ca. 200–180 Ma and ca. 130 Ma. In summary, we assume that the magmatic activity in the arc at the scale of the investigated area was nearly continuous from Latest Triassic to Latest Jurassic–Early Cretaceous considering the ages of both, volcanic and intrusive units. The present surface of the deep section of the arc was close to erosion already in the late Cretaceous according to apatite fission track ages (Maksaev 1990; Andriessen and Reutter, 1994).

Various systems of dykes crosscut the late Palaeozoic units and also late Jurassic plutonic rocks. The most prominent dike systems with a width of up to 20 m and kilometre-length have been interpreted as feeder dikes of the volcanic rocks (Pichowiak and Breitkreuz 1984). The dikes document the latest magmatic activity in the area. Dikes in this study are from the shallow section at ca. 26°S (Fig. 1b, location 21) and the previously investigated deep section of the coastal batholith at ca. 24°S (Early Cretaceous dikes; Lucassen and Franz 1994; Lucassen et al. 2002).

Chemical and isotopic compositions

Sample selection for geochemistry is a major issue in the volcanic rocks, which show abundant alteration already visible in the handspecimen. Detailed sampling of selected profiles (Bartsch 2004; Kramer et al. 2005 and references therein) provided a range of rock specimen, which enabled the selection of the most suitable samples for the various analytical methods on the basis of thin sections and XRF data. For XRF analyses a broader spectrum of variably altered to fresh samples were used in order to achieve a reasonable covering of the profiles, whereas trace element analyses were only performed on

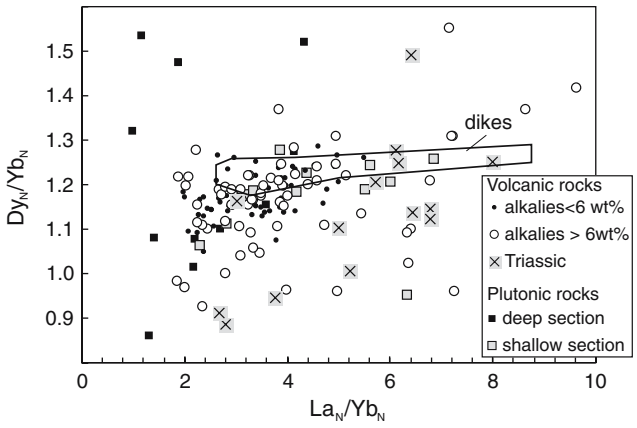

Fig. 4 Dy_n/Yb_n and La_n/Yb_n of volcanic and plutonic rocks and dikes. The ratios are low in most samples, i.e., indicate flat REE pattern and garnet-free sources and contaminants. The scatter in the rocks from the deep section is related to their cumulate character. Normalized to C1 chondrite (Sun and McDonough 1989)

moderately altered to fresh samples. Isotope analyses were performed on the least altered or fresh samples. Samples for XRF analyses were handpicked after crushing and before milling; powdered samples for trace element and isotope determination were additionally

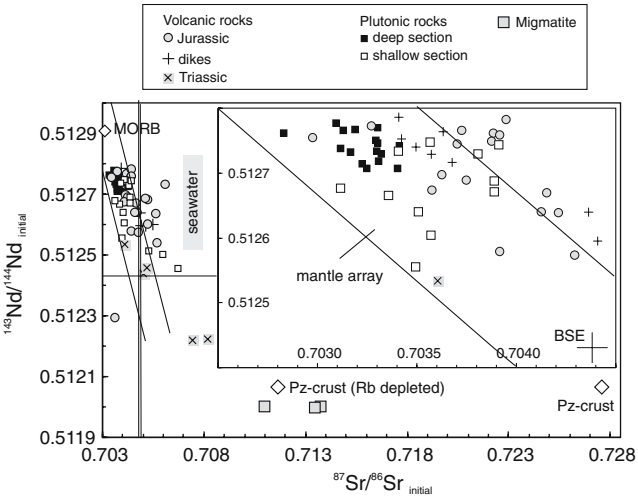

Fig. 5 Initial Sr and Nd isotopic compositions of Jurassic and Triassic volcanic rocks, dikes, and plutonic rocks. The *inset* shows the depleted quadrant only. Initial ratios of regional important reservoirs and the migmatite are shown at 160 Ma: *MORB* average Pacific MORB compiled from the Petrological Database of the Ocean Floor http://www.petdb.org; the Nd isotope ratio is corrected for in-situ decay to 160 Ma using a $^{147}Sm/^{144}Nd$ ratio of 0.214; Pz-crust = average Early Palaeozoic lower crust (Rb-depleted) and upper crust (Lucassen et al. 2001). Sr isotopic composition of bulk silicate earth (BSE) is calculated at 160 Ma assuming Rb/Sr ratio of 0.03 (McDonough & Sun 1995) and an initial $^{87}Sr/^{86}Sr$ of 0.69898 (Allegre et al. 1975). $^{87}Sr/^{86}Sr$ ratios for Jurassic seawater (0.7068–0.7074) from Veizer et al. (1997). Additional data from Lucassen et al. (2002) and Kramer et al. (2005)

treated with acetic acid to remove possible carbonate. Details of sample treatment, analytical methods, and data quality are in the electronic Appendix. In contrast to the Jurassic volcanic rocks, the samples of plutonic rocks, dikes, and Triassic volcanic rocks are not affected by alteration.

The description of bulk rock major and trace element composition of the volcanic rocks (Table A1) includes all analyses irrespective the variable degree of hydrothermal overprint, in order to give an overview of some compositional characteristics of this voluminous volcanic rocks without discussion of details of the magmatic evolution. The presentation of the isotope compositions aims to distinguish different sources in crust and mantle. The volcanic rocks for this discussion have been selected from a bigger data set (including published data), which also comprises samples with substantial metasomatism affecting the Rb/Sr and U/Pb ratios (Table A1). The Sm/Nd system is not affected by the hydrothermal alteration. The effect of this selection is reduction of the scatter introduced to the respective isotope ratios by correction for in-situ decay of samples with high Rb/Sr and U/Pb ratios and an uncertain age of alteration. Selection criteria were $H_2O + CO_2 < 3$ wt% and $CO_2 < 0.5$ wt% (all volcanic rock samples), and, $^{87}Rb/^{86}Sr < 0.3$ for calculation of Sr isotope ratios and $^{238}U/^{204}Pb < 15$ (μ ratio) for calculation of Pb isotope ratios (Table 1). Detailed account to the full data set of isotope analyses in the volcanic rocks and Rb and U metasomatism is given in the electronic Appendix

Bulk rock major element composition

The alkali and SiO_2 contents of the volcanic rocks are highly variable and range from basalt to trachydacite, but most samples are basaltic andesite and basaltic trachyandesite and represent a similar stage of magmatic evolution of presumably basaltic parental magmas (Fig. 2a). The origin of the unusually high alkalinity in many volcanic rocks will be discussed elsewhere in detail and we restrict here to the description of the composition of the alkaline rocks in comparison with the subalkaline rocks of the same arc system. The other major elements show a similar broad scatter with indicators of magmatic differentiation. The Triassic volcanic rocks comprise mainly (trachy-) dacite to rhyolite (Fig. 2). The composition of dikes from different areas is similar to the composition of many volcanic rocks and varies between subalkaline basalt and dacite, but most samples are basaltic andesite and basaltic trachyandesite (Fig. 2).

The plutonic rocks follow exclusively a calcalkaline compositional trend (Fig. 2b). The data are equally

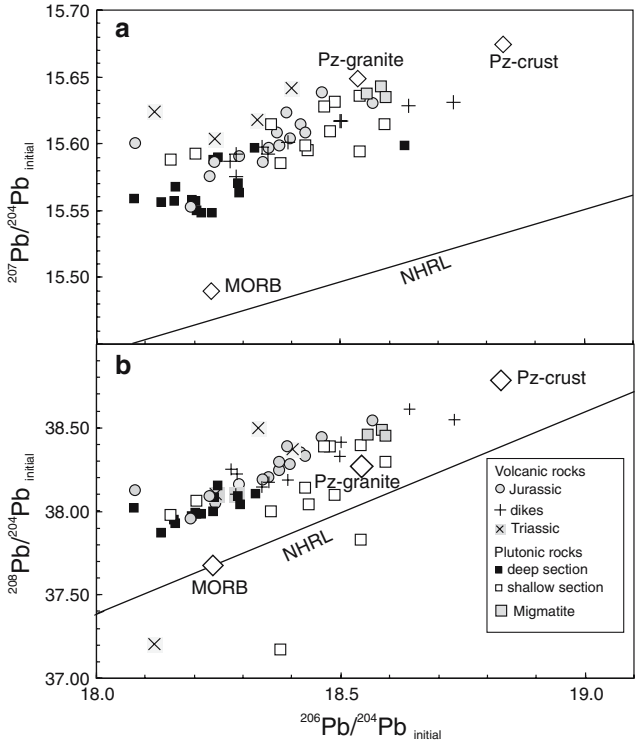

Fig. 6 Initial Pb isotopic compositions of Jurassic and Triassic volcanic rocks, dikes, and plutonic rocks. Pz–granite = average late Palaeozoic granite (feldspar data) represents a deeper section of the crust in the Coastal and Pre-Cordillera (Lucassen et al. 1999); other reservoirs as in Fig. 5; northern hemisphere reference line (NHRL; Hart 1984)

distributed over the whole range from 42 to 78 wt% SiO_2 and show no compositional cluster as the volcanic rocks (Fig. 2). The deep section of the batholith comprises gabbro to diorite. The shallow section comprises mainly quartz–dioritic and some granitic rocks, mafic compositions are rare and represent local cumulates (Fig. 2b). Many of the various intrusive units from the transition between the deep and shallow section resemble the compositional range of the shallow section, but some are similar to the gabbros and diorites of the deep section (Figs. 1b, 2b; Marinovic and Hervé 1988; Marinovic et al. 1995).

Bulk rock trace element composition

The sample set analysed for a range of trace elements includes data from this study (Table A1) and published data of our working group (Lucassen et al. 2002; Bartsch 2004; Kramer et al. 2005). Primitive mantle-normalized trace element patterns of the volcanic rocks are remarkably uniform regardless of age, geographical position or alkalinity and the main difference between the samples appears to be the absolute content of the respective elements. The large number of samples ($n = 149$) allows a statistically significant conclusion. Therefore, we present the data here as mean values (Fig. 3). The data for individual samples are in the electronic appendix (Table A1; Fig. A1). The LILE enrichment, deep Nb and Ta trough and positive Pb and negative Ti spike is typical of magmatic rocks generated in magmatic arcs including rocks from 'primitive' island arcs (e.g. Hawkesworth et al. 1993). La_n/Yb_n (2–7 most samples, all but three samples < 10) and Dy_n/Yb_n ratios (0.9–1.3 most samples; Fig. 4) indicate flat and uniform REE pattern. Eu-anomalies are absent to moderate (92% of the samples fall within a range Eu/Eu* 1.1–0.6) according to the relatively uniform degree of fractionation to basaltic andesite and andesite compositions. Normalized trace element patterns of the Triassic volcanic rocks and the dikes are similar to those of the Jurassic volcanic rocks (Figs. 3, 4).

Incompatible trace element contents in the plutonic rocks from the deep section are generally lower than in the volcanic or plutonic rocks from the shallow section, but the patterns show the same characteristics seen in the pattern of the other plutonic and volcanic rocks with a negative Nb and positive Pb spike (Fig. 3) and flat REE pattern (Fig. 4). Trace element patterns of plutonic rocks from the shallow section are generally similar to those of the volcanic rocks and the main difference between the pattern of the volcanic and plutonic rocks are higher U–Th contents of the latter (Fig. 3).

In summary, the subalkaline volcanic rocks and dikes and the plutonic rocks follow mainly a calcalkaline evolution despite their different ages and regional distribution. Trace element patterns including those of alkaline rocks are rather uniform and typical of magmatic rocks generated in a subduction zone setting (e.g. Hawkesworth et al. 1993). REE patterns preclude the presence of substantial amounts of garnet in the source of the parental magmas or at depth of assimilation of wall rock. The Fe–Mg minerals olivine, clino-, and orthopyroxene dominate the source mineralogy and the early stages of mineral fractionation. Amphibole is common only in andesite to dacite compositions. Eu/Eu* ratios are $> 0.6 \leq 1.1$ in most samples and indicate variable fractionation of plagioclase, which is present as a phenocryst in all samples. Systematic variations of major and trace element contents, which can occur regionally and locally in the volcanic rocks, contain e.g. information on variable conditions of melting of the samples (Kramer et al. 2005; Bartsch 2004), but do not affect their isotopic composition.

Radiogenic isotopes

Radiogenic isotope composition is indicative for the contribution of different sources to igneous rocks during their magmatic evolution from the source region to the final state of a specific sample. The isotopic compositions of important endmembers in the crust-mantle system at the Chilean continental margin are shown in Figs. 5 and 6. The composition of average Pacific MORB is used as approximation to the Nd, Sr, and Pb isotope composition of the large convective depleted mantle reservoir. The early Palaeozoic crust and derived sediments are the source for assimilation in magmatic processes and melt generation within the crust, the source of sediments from the continent into the trench, and the source of possible tectonically eroded material from the continent. Migmatites from the contact of the shallow plutons represent the local uppermost crust.

Most volcanic and plutonic rocks plot into the field of depleted mantle with a restricted range of initial $^{143}Nd/^{144}Nd$ (ca. 0.5125 to 0.5128) and $^{87}Sr/^{86}Sr$ ratios (ca. 0.703–0.705). This composition is different from the ambient Andean continental crust and the average Pacific MORB (Fig. 5). The isotope compositions of the plutonic rocks from the deep section are the most uniform among the different groups and show consistently the most depleted signature. Low $^{87}Sr/^{86}Sr$ initial ratios (0.7031–0.7037; Marinovic et al. 1995) of rocks from the transitional section leave no doubt that they are part of the composite batholith. The negative correlation of Nd and Sr isotope ratios defined by some samples is strongest among the Triassic volcanic rocks and indicates additions of ambient Paleozoic crust, e.g., by wall rock assimilation in the plutonic rocks from the shallow section. Samples QCA 5 to 9 represent a profile away from the contact to migmatite samples QCA 1–3 and indicate decreasing contamination with increasing distance (see Table 1). Substantial amounts of Palaeozoic crustal material are present in the composition of only very few samples. The scatter of $^{87}Sr/^{86}Sr$ at similar $^{143}Nd/^{144}Nd$ in some Jurassic volcanic rocks is attributed to seawater alteration, but none of the samples reaches the Jurassic seawater Sr isotope composition (see also discussion of metasomatism of the volcanic rocks in the electronic Appendix).

Pb isotope compositions (Fig. 6) of most samples of the plutonic rocks from the deep section fall into a small compositional field defined by $^{206}Pb/^{204}Pb$ (18.1–18.4), $^{207}Pb/^{204}Pb$ (15.55–15.60), and $^{208}Pb/^{204}Pb$ ratios (37.9–38.1), which is different from MORB and local crust composition. This compositional field is resembled by some samples of the plutonic rocks from the shallow section, the volcanic rocks and the dikes, whereas other samples show influence of the local Palaeozoic crust and few samples resemble the composition of local Palaeozoic granite and migmatite. The hybrid compositions underline the minor influence of Palaeozoic crustal material especially considering the much lower Pb contents of mafic magmas compared with those from felsic crust.

Discussion

Isotopic composition of the Mesozoic to Recent subarc mantle

The isotopic composition of the Mesozoic magmatic rocks (18°–27°) is compared with the composition of late Tertiary to Recent magmatic rocks from a section of the Southern Andes (36°–40°S; SVZ; Fig. 1a), where mantle derived magmatism (e.g. Hildreth and Moorbath 1988; Lucassen et al. 2004) continued in a near stationary magmatic arc since Jurassic (Mpodozis and Ramos 1989; Kemnitz et al. 2005). The discussion restricts to Nd and Pb isotope ratios because Sr isotopes were influenced by post-magmatic alteration (nevertheless, most $^{87}Sr/^{86}Sr$ ratios plot into the depleted mantle field). The initial Nd isotope compositions of the arc derived rocks show an upper limit of the most radiogenic values, which form two arrays with variable $^{87}Sr/^{86}Sr$ ratios within the field of depleted mantle (Fig. 7a): one with ca. 0.51277 in the Mesozoic rocks of the north is in excellent agreement with initial ratios from mineral isochrons from the same rock suite (Lucassen and Thirlwall 1998), a second one of ca. 0.5129 represents the Tertiary to Recent rocks in of the south. The initial $^{206}Pb/^{204}Pb$ ratios also show a 'normal' evolution to slightly more radiogenic compositions from the Jurassic to Recent (Fig. 7b; 18.20 in the northern, ca. 18.50 the southern section). The most radiogenic Nd and least radiogenic Pb isotope compositions are considered as the best approximation to the isotope composition of the subarc mantle in the Jurassic and late Cenozoic, respectively. The correlation of Nd and Sr isotope ratios and of the $^{206}Pb/^{204}Pb$ and $^{207}Pb/^{204}Pb$ ratios in both sections is explained by the addition of small amounts of the ambient old crustal material during magma evolution within the crust (Fig. 7b), but some contribution to the scatter could equally origin from small heterogeneities in the mantle source. The two datasets indicate generally similar compositions of the subarc mantle source, with slightly more radiogenic isotope compositions in the younger southern section and a similarly minor

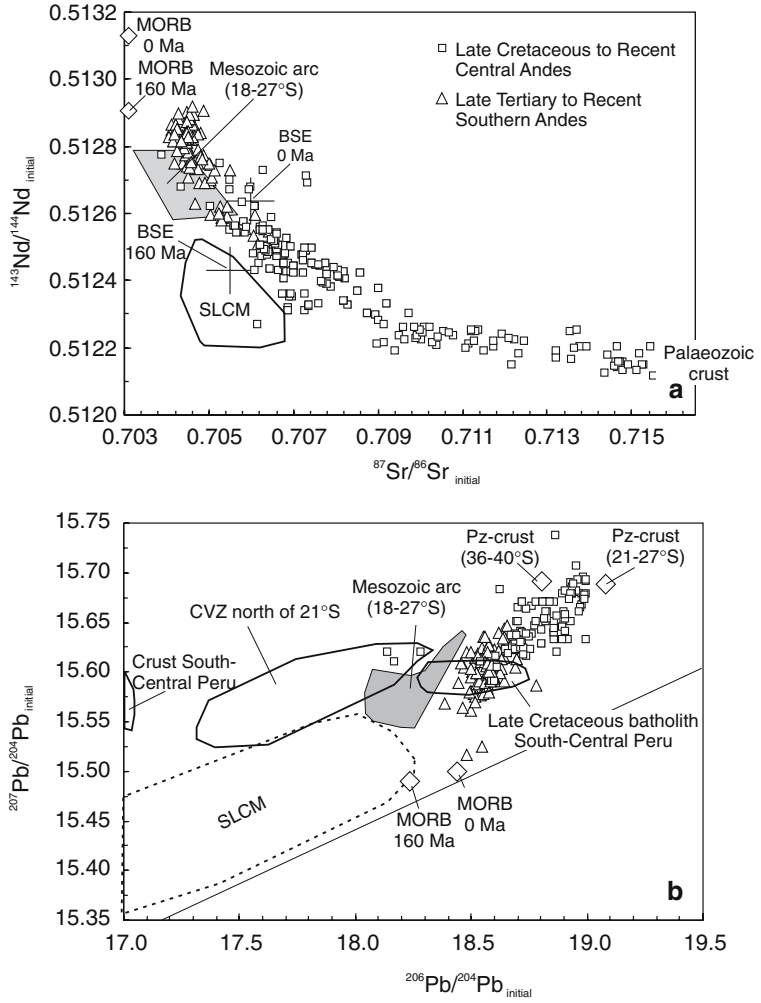

Fig. 7 Comparison of **a** Nd and Sr and **b** Pb isotopic composition of Mesozoic igneous rocks (18°–27°S; grey shaded field), Late Tertiary to Recent igneous rocks of the Southern (36°–40°S), Late Cretaceous to Recent igneous rocks of the Central Andes, Pb isotope composition of the Late Cretaceous batholith of Southern-Central Peru, and regional crust and mantle reservoirs. Data sources: Tertiary to Recent igneous rocks (36°–40°S) and Cenozoic igneous rocks of the Central Andes were compiled from GEOROC data base (http://www.georoc.mpch-mainz.gwdg.de/georoc); Late Cretaceous and Tertiary rocks of the Central Andes: Rogers and Hawkesworth (1989) and Haschke et al. (2002); CVZ Cenozoic volcanic rocks north of 21°S: Aitcheson et al. (1995); crust and batholith of South-Central Peru : Mukasa and Tilton (1985); SLCM is the subcontinental mantle of the Proterozoic Brazilian shield: Carlson et al. (1996) Gibson et al. (1996), Marques et al. (1999), Lucassen et al. (2002), unpublished data of F. Lucassen; average Pz-crust (36°–40°S) from Lucassen et al. (2004): other data sources see Figs. 5 and 6

influence of crustal contamination in both sections. If we accept the least crust contaminated and most 'depleted' isotopic compositions of the Jurassic arc as the initial composition of the subarc mantle in the Jurassic, the difference of the Nd and Pb isotope compositions between the two sections of different age could be described by 160 Myr of radiogenic growth with—compared to MORB type depleted mantle—enriched Nd and U resulting in lower $^{147}Sm/^{144}Nd$ ratio of ~ 0.15 and a higher μ of ~ 12, respectively. In other areas of the Mesozoic to Early Tertiary arc in Chile (27–36°S), Nd, Sr, (Vergara et al., 1995; Parada et al. 1999; Marschik et al. 2003; Nyström et al. 1993, 2003) and Pb isotope compositions (Marschik et al. 2003; Nyström et al. 2003) fit into this scheme.

The isotopic uniformity of the subarc mantle can be tested further by comparison of the isotopic composition between the inferred subarc mantle and hybrid Late Cretaceous to Recent magmas from the northern section. The variation of the Nd and Sr isotope composition in the Andean Late Mesozoic to Recent magmatic rocks is sufficiently described by mixing of the inferred subarc mantle composition and the ambient old continental crust (Fig. 7a). The contributions of

the crust to the arc magmas increase with the building of the Cenozoic Andes, i.e. the thickening of the crust especially in the region of the Andean Plateau north of 27°S (CVZ in Fig. 1a), which was established in numerous investigations of the chemical and isotopic composition of the Cenozoic Andean magmatism. Pb isotope ratios are specifically sensitive to addition of crust to mantle derived magmas due to a large difference in the Pb contents, which is high in the crust, and in many cases different Pb isotope compositions of crust and mantle. Pb isotope compositions of Cenozoic volcanic rocks from the CVZ show different Pb isotope compositions south and north of ca. 21°S (Fig. 7b), which were interpreted as the influence of different Pb provinces within the (lower) crust and assigned to inherited heterogeneity of the Early Palaeozoic to Proterozoic basement (e.g. McFarlane et al. 1990; Wörner et al. 1994; Aitcheson et al. 1995). Such Pb isotope variations (Fi.7b) are not seen in Jurassic volcanic rocks north of 21°S (Kramer et al., 2005; this work). They are also absent in the Cretaceous Coastal Batholith of southern and central Peru, which intruded into Proterozoic basement with characteristic Pb signatures (Fig. 7b; Mukasa and Tilton 1985). Together with other evidence for an upper mantle source of the Peruvian Batholith Mukasa and Tilton (1985) concluded from the near identical Pb isotope compositions of arc magmatism in Central Chile and their batholith samples that the crustal contributions were minor and the Pb isotope compositions dominated by the composition of the subarc mantle source.

In summary, the observations suggest a compositional homogeneity of the Sm–Nd and U–Pb isotope systems (and Rb–Sr system) in the subarc mantle on a large time and regional scale. The composition of the subarc mantle is different from the composition of a typical depleted asthenospheric reservoir such as sampled by Pacific MORB. The composition of the magmatic rocks from the subarc mantle also indicates no substantial contributions of the old subcontinental mantle beneath the Brazilian Shield (Fig. 7). The latter was proposed as a potentially important mantle source during ongoing shortening in the Cenozoic Andean orogen (e.g. Rogers and Hawkesworth 1989).

Volume of the Mesozoic magmatism

The generally mafic to intermediate compositions and the—at the given large scale of the investigation—uniform isotope signatures of the widely distributed sample areas indicate mainly juvenile additions to the crust in the Mesozoic magmatic arc. The overall volume of the Mesozoic magmatic additions (18–27°S) is difficult to estimate, because the Mesozoic arc continues off shore and is partly eroded. Geophysical data show a high velocity—high density structure in the Coastal area 21°–24°S extending toward the trench and ca. 70 km from the cost line inland (e.g. Götze and Kirchner 1997; Wigger et al. 1994; Kösters 1999; Schmitz et al. 1999; Oncken et al. 2003), which was interpreted as prevailing juvenile mafic to intermediate magmatic crust (e.g. Lucassen et al. 1996). We infer a similar crustal structure for the whole investigated section based on the geochemical similarity of the rocks. Assuming a width of outcropping plutonic and volcanic rocks of 50–100 km and a thickness of at least 25 km (from geophysical data) the minimum magmatic addition is 1,250–2,500 km^3 in 60 Myr per km N–S extension of the arc. There are no tight constraints whether the Mesozoic magmatism was continuous or periodically enhanced, but we infer a near continuous magmatic activity from the age record of the plutonic and volcanic rocks and the longstanding thermal anomaly within the crust of the arc (Lucassen et al. 1996; Scheuber and Gonzales 1999). Assuming a continuous activity over ca 60 Ma, the average productivity was 20–40 km^3/(km Myr) and is within lower to mid-range of average production rates of island arcs (Dimalanta et al. 2002). The cumulative volume of the Mesozoic igneous rocks along the studied section (18–27°S, ca. 1,000 km) is $1.25–2.5\times10^6$ km^3.

Voluminous arc magmatism also occurs in the southern and northern continuation of our study area. Early to Late Jurassic magmatism with dominant basaltic-andesite composition was reported (Romeuf et al. 1993, 1994 and references therein) from southern and central Peru, but detailed geochemical studies are not available. These rocks represent most likely the continuation of the Mesozoic arc towards the north. The Coastal area of central and northern Peru was the location of intense mantle derived magmatism from Cretaceous to Early Tertiary comprising abundant basalt to basaltic-andesite compositions, which extruded and intruded into N–S extended basin structures (e.g. Atherton et al. 1983; contributions in Pitcher et al. 1985). These rocks form a high-density anomaly at crustal scale in the geophysical image of the crust (Atherton et al. 1983; Haederle and Atherton 2002). South of our study area, in Central Chile, mantle derived magmatism starts in the Jurassic and formed a large magmatic province mainly of Early Cretaceous age (e.g. Vergara et al. 1995). Bohm et al. (2002) observed in the Mesozoic to Recent crust (36–40°S) similarly high seismic velocities as known at ca. 24°S. These high velocities have been interpreted to be caused by mafic to intermediate intrusions. Although

no cumulative volume estimates for the above volcanic and plutonic rocks have been published, the volumes of juvenile additions in the above sections are likely comparable to those from 18–27°S, which is supported by the large aerial distribution of volcanic and intrusive rocks and their prominent appearance in the geophysical image.

Juvenile magmatism and tectonic regime

One of the most intriguing observations in the Mesozoic arc is the emplacement and preservation of the large volume of juvenile mafic to intermediate rocks in the old continental crust without major contributions of the latter. The following is exemplified for the Chilean margin of the Central Andes, but should be equally valid for comparable settings. The regime of tectonic extension to transtension and occasional transpression are the dominant tectonic styles in the Mesozoic Chilean arc and persisted at least from the late Triassic to late Cretaceous. The extension was triggered by oblique plate configurations causing oblique subduction in Chile (e.g. Scheuber et al. 1994; Franzese and Spalletti 2001; Grocott and Taylor 2002). Extension favours the emplacement of plutonic rocks within the mid and upper crust (e.g. Glazner 1991; Grocott and Taylor 2002) and could also have enabled the ascent of dense mafic melts into the mid crust as observed in the deep section of the arc at ca. 24°S and inferred elsewhere from the geophysical image of the crust. Volcanic rocks, which were deposited in extensional structures, remained close to the sea level throughout the deposition of the thick piles of volcanic rocks (e.g. Vergara et al. 1995; Bartsch 2004; Kramer et al. 2005). They erupted along fissures, an eruption style typical for extensional (or non-compressional) settings, e.g. continental flood basalts or volcanism in extensional back-arcs. Throughout the late Palaeozoic and Mesozoic, the crustal thickness has been close to normal, without the creation of a large relief, and thus without significant exhumation. The mid-crustal section of the arc south of Antofagasta seems to be the only exception (ca. 24°S; e.g. Scheuber and Gonzales 1999).

A second important characteristic of the Mesozoic arc is the longstanding stability of the arc, which probably exceeded 60 Myr, because already late Palaeozoic and Triassic magmatism occurred in the same area. The compositional effect of such a stationary position (or oscillation) alone is increasing hybridization of the composition of the pre-existing crust with each magma pulse added from the mantle (which is already traceable as a process at a much shorter time-scale in single volcanoes of the Cenozoic Central Andes; e.g. Feeley 1993). Heating of the crust in the late Palaeozoic arc activity produced granites with high proportions of re-molten crust, and fusible minerals such as micas were likely exhausted (Lucassen et al. 1999; Morata et al. 2000). The crustal component in arc magmatism of northern Chile increases again in Late Cretaceous and Early Tertiary magmatic rocks of northern Chile (e.g. Rogers and Hawkesworth 1989; Haschke et al. 2002), after the arc started moving eastward on Palaeozoic crust of near-normal thickness, in which the fusible minerals were not yet exhausted.

Intrusion and extrusion of juvenile magmas continue up to Recent, where at least one of the favourable conditions—tectonic extension or stationary position of the arc—persisted. In the southern section, at ca. 36°–40°S the arc is near stationary since Jurassic (Mpodozis and Ramos 1989; Kemnitz et al. 2005) and despite the actual contractional tectonic regime the isotopic compositions of the present magmatism are still reflecting the composition of the subarc mantle.

Conclusions

The Jurassic–Early Cretaceous magmatic arc was a major site of juvenile intermediate to mafic additions to the old crust of the continental arc, which appears to be unique in the Phanerozoic history of the Central Andes. Compositional uniformity and cumulative volume of volcanic and plutonic rocks produced a large magmatic province related to an active continental margin. The preserved volume of juvenile rocks is comparable to the volumes of LIPs, but the magmatic activity is distributed over a much longer time than in a LIP. A major requisite for the formation and preservation of new mafic to intermediate crust in the Mesozoic arc is not an exceptionally high average productivity of magmas in the arc, which seems to be within the normal range of magmatic arcs, but the long-standing oblique subduction at a non-accretionary margin triggering extensional tectonics. Extensional tectonics favoured the emplacement of the magmas in those parts of the crust, where a preservation of the magmatic additions is more likely than in others. The plutons intruded into extensional structures within the mid and upper crust, are thus more easily exposed and due to the fact that the crust was not thickened, less differentiated than in the Cenozoic arc. There is no direct information from the lower crust, but it is mafic from geophysical evidence. The volcanic rocks extruded into subsiding basins, i.e. the morphological elevation of the arc was close to sea level. Erosion is

less important than in the Cenozoic high Andes and thick piles of volcanic rocks were preserved. In contrast, compressional tectonic settings at active continental margins favour the formation of thick mafic keels at the base of the continental crust by magmatic underplating, which are prone to gravitational instability and commonly removed by delamination (e.g. Meissner and Mooney 1998). The high morphologies above sea level, which expose the volcanic deposits, strongly contribute to their erosion.

The uniform isotopic composition of the subarc mantle in the Mesozoic and its evolution to an equally uniform only slightly different present composition must have consequences for the composition of the asthenospheric mantle reservoir linked to the convective mantle wedge. The similar major element composition of the primary arc magmas over the long period of activity of the Andean arc requires continuous replenishment of the melting zone in the mantle wedge by 'fresh' asthenosphere (e.g. Thorpe et al. 1981) and, hence, the return of the residue to a reservoir. This reservoir is most likely located beneath the continent, because the continuous subduction of the cold oceanic lithosphere beneath the Andean margin separates continental and oceanic asthenosphere. The isotopic composition in the melt region of the mantle wedge, i.e., in the potential residue, should be very similar to the composition of the melt. There are no constraints on the isotopic composition of the 'fresh' asthenosphere and we only know the compositions of the magmas from the subarc mantle. Assuming an isotopic composition of MORB type depleted mantle for the 'fresh' asthenosphere the observed composition of arc magmas could reflect well-balanced mixing within the mantle wedge of ageing MORB type depleted mantle with melts or fluids from ageing reservoirs. These reservoirs are altered oceanic crust and sediments and subducted continental crust (sediments and tectonically eroded material) with less radiogenic Nd and more radiogenic Pb and Sr signatures. The fate of the returned residue in the subcontinental asthenosphere is unknown, but the process, which produces mantle of distinct but uniform composition, is active at least since 200 Ma and may have modified the composition of the asthenosphere reservoir connected with the mantle wedge.

Acknowledgements We thank Anette Meixner, Rudolf Naumann, Cathrin Schulz, and Christa Wiesenberg for their assistance in the GFZ-Potsdam laboratories; Maren Lewerenz for sample preparation and XRF analysis at TU-Berlin. Jörg Binas is thanked for samples from the Argolla area. Sebastian Tappe and Gerhard Wörner provided the reviews, which vastly improved the presentation of the paper. This work was financed by DFG within the Sonderforschungbereich (SFB) 267, Deformationsprozesse in den Anden.

References

Aguirre L, Féraud G, Morata D, Vergara M, Robinson D (1999) Time interval between volcanism and burial metamorphism and rate of basin subsidence in a Cretaceous Andean extensional setting. Tectonophysics 313:433–444

Aitcheson SJ, Harmon RS, Moorbath S, Schneider A, Soler P, Soria-Escalante E, Steele G, Swainbank I, Wörner G (1995) Pb isotopes define basement domains in the Altiplano, central Andes. Geology 23:555–558

Allegre CJ, Birck JL, Fourcade S, Semet MP (1975) Rubidium–87/strontium–87 age of Juvinas basaltic achondrite and early igneous activity in the solar system. Science 187:436–438

Andriessen PAM, Reutter KJ (1994) K–Ar and fission track mineral age determination of igneous rocks related to multiple arc systems along the 23°S latitude of Chile and NW Argentina. In: Reutter KJ, Scheuber E, Wigger PJ (eds) Tectonics of the Southern Central Andes. Springer, Berlin Heidelberg New York, pp 141–153

Ardill J, Flint S, Chong G, Wilke H (1998) Sequence stratigraphy of the Mesozoic Domeyko Basin, northern Chile. J Geol Soc (Lond) 155:71–88

Atherton MP, Pitcher WS, Warden V (1983) The Mesozoic marginal basin of central Peru. Nature 305:303–306

Bartsch V (2004) Magmengenese der obertriasssischen bis unterkretazischen Vulkanite in der Küstenkordillere von Nord-Chile zwischen 24° und 27°S. Doctoral Dissertation; Technical University of Berlin, School of Civil Engineering and Applied Geosciences, 2004–07–14 http://www.edocs.tu-berlin.de/diss/2004/bartsch_viola.pdf (in German)

Bebiolka A (1999) Eine obertriassische Flora aus der nordchilenischen Küstenkordillere (Agua Chica Formation, Quebrada Pan de Azùcar). Neues Jahrbuch Geologie Paläontologie Abhandlungen 211:213–232

Berg K, Baumann A (1985) Plutonic and metasedimentary rocks from the Coastal range of northern Chile: Rb–Sr and U–Pb isotopic systematics. Earth Planet Sci Lett 75:101–115

Bock B, Bahlburg H, Wörner G, Zimmermann U (2000) Tracing crustal evolution in the Southern Central Andes from Late Precambrian to Permian with geochemical and Nd and Pb isotope data. J Geol 108:515–535

Bohm M, Lüth S, Echtler H, Asch G, Bataille K, Bruhn C, Rietbrock A, Wigger P (2002) The Southern Andes between 36°–40° latitude: seismicity and average seismic velocities. Tectonophysics 356:275–289

Buchelt M, Zeil W (1986) Petrographische und geochemische Untersuchungen an jurassischen Vulkaniten der Porphyrit-Formation in der Küstenkordillere Nord-Chiles. Berliner Geowissenschaftliche Abhandlungen 66:191–204

Buchelt M, Tellez C (1988) The Jurassic La Negra formation in the area of Antofagasta, northern Chile (lithology, petrography, geochemistry). In: Bahlburg H, Breitkreuz C, Giese P (eds) The southern Central Andes. Lecture notes in earth sciences, vol 17, Springer, Berlin Heidelberg New York, pp 172–182

Carlson RW, Esperanca S, Svisero DP (1996) Chemical and Os isotopic study of Cretaceous potassic rocks from southern Brazil. Contrib Mineral Petrol 125:393–405

Clarke KD (1998) Geología, petrografía y geoquímica de las rocas intrusivas de la Cordillera de la Cost entre Paposo y Taltal. unpublished MSc Thesis, Universidad Catolica del Norte, Department de Geologia, Antofagasta, p 175

Coffin MF, Eldholm O (1994) Large igneous provinces: crustal structure, dimensions, and external consequences. Rev Geophys 32:1–36

Coira B, Davidson J, Mpodozis C, Ramos V (1982) Tectonic and magmatic evolution of the Andes of northern Argentina and Chile. Earth Sci Rev 18:303–332

Cordani UG, Sato K, Teixeira W, Tassinari CCG, Basei MAS (2000) Crustal evolution of the South American platform. In: Cordani UG, Milani EJ, Thomaz Fihlo A, Campos DA (eds) Tectonic evolution of South America. Rio De Janeiro, pp 19–40

Dallmeyer RD, Brown M, Grocott J, Taylor GK, Treloar PJ (1996) Mesozoic magmatic and tectonic events within the Andean plate boundary zone, 26°–27°30′S, North Chile: constraints from $^{40}Ar/^{39}Ar$ mineral ages. J Geol 104:19–40

Damm KW, Harmon RS, Kelley S (1994) Some isotope and geochemical constraints on the origin and evolution of the Central Andean basement (19°–24°S). In: Reutter KJ, Scheuber E, Wigger PJ (eds) Tectonics of the Southern Central Andes. Springer, Berlin Heidelberg New York, pp 263–275

Dimalanta C, Taira A, Yumul Jr GP, Tokuyama H, Mochizuki K (2002) New rates of western Pacific island arc magmatism from seismic and gravity data. Earth Planet Sci Lett 202:105–115

Ernst WG (2000) Earth systems; processes and issues. Cambridge University Press, Cambridge, pp 566

Feeley TC (1993) Crustal modification during subduction-zone magmatism: evidence from the southern Salar de Uyuni region (20°–22°S), Central Andes. Geology 21:1019–1022

Francis PW, Hawkesworth CJ (1994) Late Cainozoic rates of magmatic activity in the Central Andes and their relationship to continental crust formation and thickening. J Geol Soc Lond 151:845–854

Franzese JR, Spalletti LA (2001) Late Triassic–early Jurassic continental extension in southwestern Gondwana: tectonic segmentation and pre-break-up rifting. J South Am Earth Sci 14:257–270

Gibson SA, Thompson RN, Dickin AP, Leonardos OH (1996) Erratum to 'High-Ti and low-Ti mafic potassic magmas: key to plume-lithosphere interaction and continental flood-basalt genesis'. Earth Planet Sci Lett 141:325–341

Glazner AF (1991) Plutonism, oblique subduction and continental growth: an example from the Mesozoic of California. Geology 19:784–786

Gonzales G (1996) Evolucíon tectonica de la Cordillera de la Costa de Antofagasta (Chile). Con especial referencia al los deformaciones sinmagmaticas del Jurasico—Cretacico inferior. Berliner Geowissenschaftliche Abhandlungen 181, Berlin, p 111

Götze H-J, Kirchner A (1997) Interpretation of gravitiy and geoid in the Central Andes between 20° and 29°S. J South Am Earth Sci 10:179–188

Grocott J, Taylor GK (2002) Magmatic arc fault systems, deformation partitioning and emplacement of granitic complexes in the Coastal Cordillera, north Chilean Andes (25°30′S to 27°00′S). J Geol Soc Lond 159:425–442

Gröschke M, Hillebrandt Av, Prinz P, Quinzio LA, Wilke H-G (1988) Marine Mezozoic Paleogeography in northern Chile 21°–26°S. In: Bahlburg H, Breitkreuz C, Giese P (eds) The Southern Central Andes. Lecture Notes in Earth Sciences, vol 17. Springer, Berlin Heidelberg New York, pp 71– 86

Haederle M, Atherton MP (2002) Shape and intrusion style of the Coastal Batholith, Peru. Tectonophysics 345:17–28

Hart SR (1984) A large-scale isotope anomaly in the southern hemisphere mantle. Nature 309:753–757

Haschke M, Siebel W, Günther A, Scheuber E (2002) Repeated crustal thickening and recycling during the Andean orogeny in north Chile (21°–26°S). J Geophys Res Solid Earth 107. DOI 10.1029/2001JB000328

Hawkesworth CJ, Gallagher K, Hergt JM, McDermott F (1993) Mantle and slab contributions in arc magmas. Annu Rev Earth Planet Sci 21:175–204

Hervé M, Marinovic N (1989) Geocronologia y evolución del batolito Vicuña Mackena, Cordillera de la Costa, Sur de Antofagasta (24–25°S). Revista Geologica Chile 16:41–39

Hildreth W, Moorbath S (1988) Crustal contributions to arc magmatism in the Andes of Central Chile. Contrib Mineral Petrol 98:455–489

Hillebrandt Av, Bartsch V, Bebiolka A, Kossler A, Kramer W, Wilke H-G, Wittmann, S (2000) The paleogeographic evolution in a volcanic-arc/back-arc setting during the Mesozoic in northern Chile. Zeitschrift für Angewandte Geologie SH1 2000, Hannover, pp 87–93

Kemnitz H, Kramer W, Rosenau M (2005) Jurassic to Tertiary tectonic, volcanic, and sedimentary evolution of the Southern Andean intra-arc zone. Chile (38–39°S): a survey. N Jahrbuch Geologie Paläontologie Abhandlungen 236:19–42

Kossler A (1998) Der Jura in der Küstenkordillere von Iquique (Nordchile)—Paläontologie, Lithologie, Stratigraphie, Paläogeographie. Berliner Geowissenschaftliche Abhandlungen 197, Berlin, p 226

Kösters M (1999) 3D-Dichtemodellierung des Kontinentalrandes sowie quantitative Untersuchungen zur Isostasie und Rigidität der Zentralen Anden (20°–26°S). Berliner Geowissenschaftliche Abhandlungen 32, Berlin, p 181

Kramer W, Siebel W, Romer RL, Haase G, Zimmer M, Ehrlichmann R (2005) Geochemical and isotopic characteristics and evolution of the Jurassic volcanic arc between Arica (18°30′S) and Tocopilla (22°S), North Chilean Coastal Cordillera. Chemie der Erde 65:47–78

Le Maitre RW (1989) A classification of igneous rocks and glossary of terms. Blackwell, London, p 139

Levi B, Aguirre L, Nyström JO, Padilla H, Vergara M (1989) Low-grade regional metamorphism in the Mesozoic–Cenozoic volcanic sequences of the Central Andes. J Metamorphic Geol 7:487–495

Lucassen F, Franz G (1994) Arc related Jurassic igneous and metaigneous rocks in the Coastal Cordillera of northern Chile/region Antofagasta. Lithos 32:273–298

Lucassen F, Franz G (1996) Magmatic arc metamorphism: petrology and temperature history of metabasic rocks in the Coastal Cordillera of Northern Chile/Region Antofagasta. J Metamorphic Geol 4:249–265

Lucassen F, Thirlwall MF (1998) Sm–Nd formation ages and mineral ages in metabasites from the Coastal Cordillera, northern Chile. Geol Rundschau 86:767–774

Lucassen F, Becchio R (2003) Timing of high-grade metamorphism: Early Paleozoic U–Pb formation ages of titanite indicate long-standing high-T conditions at the western margin of Gondwana (Argentina, 26–29°S). J Metamorphic Geol 21:649–662

Lucassen F, Fowler CMR, Franz G (1996) Formation of magmatic crust at the Andean continental margin during early Mesozoic: a geological and thermal model of the North Chilean Coast Range. Tectonophysics 262:263–279

Lucassen F, Franz G, Thirlwall MF, Mezger K (1999) Crustal recycling of metamorphic basement: Late Paleozoic granites of the Chilean Coast Range and Precordillera at ~ 22°S. J Petrol 40:1527–1551

Lucassen F, Becchio R, Wilke HG, Thirlwall MF, Viramonte J, Franz G, Wemmer K (2000) Proterozoic-Paleozoic development of the basement of the Central Andes (18°–26°)—a mobile belt of the South American craton. J South Am Earth Sci 13:697–715

Lucassen F, Becchio R, Harmon R, Kasemann S, Franz G. Trumbull R, Wilke H-G, Romer RL, Dulski P (2001) Composition and density model of the continental crust at an active continental margin—the Central Andes between 21°and 27°S. Tectonophysics 341:195–223

Lucassen F, Escayola M, Franz G, Romer RL, Koch K (2002) Isotopic composition of Late Mesozoic basic and ultrabasic rocks from the Andes (23–32°S)—implications for the Andean mantle. Contrib Mineral Petrol 143:336–349

Lucassen F, Trumbull R, Franz G, Creixell Ch, Vasquez P, Romer RL, Figueroa O (2004) Distinguishing crustal recycling and juvenile additions at active continental margins: The Paleozoic to Recent compositional evolution of the Chilean Pacific margin (36–41°S). J South Am Earth Sci 17:103–119

Maksaev V (1990) Metallogeny, geological evolution, and thermochronology of the Chilean Andes between latitudes 21° and 26° south, and the origin of the major porphyry copper deposits. Unpublished PhD Thesis, Dalhouse University

Marinovic N, Herve M (1988) El batolito Vicuna Mackenna. V Congreso Geologico Chileno, Tomo III, Santiago de Chile, pp 1297–1319

Marinovic N, Smoje I, Maksaev V, Hervé M, Mpodozis C (1995) Hoja Aguas Blancas. Carta Geologica de Chile No 70, Servicio Nacional de Geologia y Mineria, Santiago de Chile, p 142

Marques LS, Dupré B, Piccirillo EM (1999) Mantle source compositions of the Paraná Magmatic Province (southern Brazil): evidence from trace element and Sr–Nd–Pb isotope geochemistry. J Geodynam 28:439–458

Marschik R, Fontignie D, Chiarardia M, Voldet P (2003) Geochemical and Sr–Nd–Pb–O isotope composition of granitoids of the Early Cretaceous Copiapó plutonic complex (27°30′S), Chile. J South Am Earth Sci 16:381–398

McDonough WF, Sun SS (1995) The composition of the Earth. Chem Geol 120:223–253

Mcfarlane AW, Marcet P, LeHursa A, Petersen U (1990) Lead isotope provinces of the central Andes inferred from ores and crustal rocks. Econ Geol 85:1857–1880

Meissner R, Mooney W (1998) Weakness of the lower continental crust: a condition for delamination, uplift and escape. Tectonophysics 296:47–60

Morata D, Aguirre L Oyarzún M Vergara M (2000) Crustal contribution in the genesis of the bimodal Triassic volcanism from the Coastal Range, central Chile. Revista Geológica Chile 27:83–98

Morata D, Aguirre L (2003) Extensional Lower Cretaceous volcanism in the Coastal Range (29°20′–30°S), Chile: geochemistry and petrogenesis. J South Am Earth Sci 16:459–476

Mpodozis C, Ramos V (1989) The Andes of Chile and Argentina. In: Ericksen GE, Cañas Pinochet MT, Reinemund JA (eds) Geology of the Andes and its relation to hydrocarbon and mineral resources: Circum-Pacific Council for Energy and Mineral Resources Earth Science Series, vol 11, Houston, pp 59–90

Mukasa SB, Tilton JR (1985) Pb isotope systematics as a guide to crustal involvement in the generation of the Coastal Batholith, Peru. In: Pitcher WS, Atherton MP, Cobbing EJ, Beckinsale RD (eds) Magmatism at a plate edge: the Peruvian Andes, Blackie & Son Ltd, Glasgow, pp 235–238

Naranjo JA, Puig A (1984). Hojas Taltal y Chañaral. Carta Geologica de Chile No 62, 63. Servicio Nacional de Geologia y Mineria, Santiago de Chile, p 140

Németh K, Breitkreuz C, Wilke H-G (2004) Volcano-sedimentary successions within an intra-arc related Jurassic Large Igneous Province (LIP): La Negra Formation, Northern Chile (a preliminary scientific report on the Br 997/22–1 DFG Pilot Project).A Magyar Államy Földtani Intézet Evi Jelentése 2002 (2002 annual report of the Geological Institute of Hungary); Budapest, pp 233–256

Nyström JO, Parada MA, Vergara M (1993) Sr–Nd isotopic composition of Cretaceous to Oligocene volcanic rocks in central Chile: a trend towards MORB signature with time. II. In: International Symposium on Andean Geodynamics ISAG-93:411–414

Nyström JO, Vergara M, Morata D, Levi B (2003) Tertiary volcanism during extension in the Andean foothills of central Chile (33°15′–33°45′S). GSA Bulletin 115:1523–1537#

Oncken O and the ANCORP working group (2003) Seismic imaging of a convergent continental margin and plateau in the central Andes (Andean Continental Research Project 1996 (ANCORP′96)). J Geophys Res 108. DOI 10.1029/2002JB001771

Palacios MC (1978) The Jurassic Paleovolcanism in Northern Chile. Dissertation, Eberhard-Karls-Universität Tübingen

Pankhurst RJ, Rapela CW (1998) The Proto-Andean margin of Gondwana. Geological Society, London, Special Publications, vol 142, p 383

Parada MA, Nyström JO, Levi B (1999) Multiple sources for the coastal Batholith of central Chile (31–34°S): geochemical and Sr–Nd isotopic evidence and tectonic implications. Lithos 46:505–521

Pichowiak S (1994) Early Jurassic to Early Cretaceous magmatism in the coastal Cordillera and the Central Depression of north Chile. In: Reutter KJ, Scheuber E, Wigger PJ (eds) Tectonics of the Southern Central Andes. Springer, Berlin Heidelberg New York, pp 203–218

Pichowiak S, Breitkreuz C (1984) Volcanic dykes in the North Chilean coast Range. Geologische Rundschau 73:853–863

Pitcher WS, Atherton MP, Cobbing EJ, Beckinsale RD (1985) Magmatism at a plate edge the Peruvian Andes. Blackie & Son Ltd, Glasgow, p 328

Prinz P, Wilke H-G, Hillebrandt Av (1994) Sediment accumulation and subsidence history in the Mesozoic marginal basin of northern Chile. In: Reutter KJ, Scheuber E, Wigger PJ (eds) Tectonics of the Southern Central Andes. Springer, Berlin Heidelberg New York, pp 219–232

Reutter KJ, Döbel R, Bogdanic T, Kley J (1994). Geological map of the Central Andes between 20°S and 26°S (1:1,000,000). In: Reutter KJ, Scheuber E, Wigger PJ (eds) Tectonics of the Southern Central Andes. Springer, Berlin Heidelberg New York

Rogers G, Hawkesworth CJ (1989) A geochemical traverse across the North Chilean Andes: evidence for crust generation from the mantle wedge. Earth Planet Sci Lett 91:271–285

Romeuf N, Aguirre L, Carlier G, Soler P, Bonhomme M, Elmi S, Salas G (1993) Present knowledge of the Jurassic volcanogenic formations of southern coastal Peru. In: Second international symposium andean geodynamics, Oxford 1993:437–440

Romeuf N, Aguirre L, Soler P, Carlier G, Féraud G, Jaillard E, Ruffet G (1994) Middle Jurassic volcanism in the Northern (Ecuador and Northern Peru) and Central (Peru) Segments of the Andes. In: 7th Congreso Geologico Chileno Concepcion 1994, Actas II:1438–1442

Rössling R (1989) Petrologie in einem tiefen Krustenstockwerk des jurassischen magmatischen Bogens in der nord-chilenischen Küstenkordillere südlich von Antofagasta. Berliner Geowissenschaftliche Abhandlungen 112:73

Sato K, Siga O (2002) Rapid growth of continental crust between 2.2 and 1.1 Ga in the South American Platform: Integrated Australian, European, North American and SW USA crustal evolution study. Gondwana Res 5:165–173

Scheuber E, Bogdanic T, Jensen A, Reutter KJ (1994) Tectonic development of the North Chilean Andes in relation to plate convergence and magmatism since the Jurassic. In: Reutter KJ, Scheuber E, Wigger PJ (eds) Tectonics of the Southern Central Andes. Springer, Berlin Heidelberg New York, pp 7–22

Scheuber E, Gonzales G (1999) Tectonics of the Jurassic–Early Cretaceous magmatic arc of the north Chilean Coastal Cordillera (22–26°S): a story of crustal deformation along a convergent plate boundary. Tectonics 18:895–910

Schmitz M, Lessel K, Giese P, Wigger P, Araneda M, Bribach J, Graeber F, Grunewald S, Haberland C, Lüth S, Röwer P, Ryberg T, Schulze A (1999) The crustal structure beneath the Central Andean forearc and magmatic arc as derived from seismic studies—the PISCO 94 experiment in northern Chile (21°–23°S). J South Am Earth Sci 12:237–260

Schobbenhaus C, Bellizzia A coordinators (2001) Geological Map of South America, 1:5,000,000. CGMW.CPRM-DNPM-UNESCO, Brasilia

Suarez M, Bell CM (1992) Triassic rift-related sedimentary basins in northern Chile (24°–29°S). J South Am Earth Sci 6:109–121

Sun S, McDonough WF (1989) Chemical and Isotopic Systematics of oceanic basalts: implications for Mantle composition and processes. In: Saunders AD, Norry MJ (eds) Magmatism in the Ocean Basins. Special publication Geological Society of London 42:313–345

Tankard AJ, Uliana MA, Welsink HJ, Ramos VA, Turic M, Franca AB, Milani EJ, de-Brito-Neves BB, Eyles N, Skarmeta J, Santa-Ana H, Wiens F, Cirbian M, Paulsen OL, Germs GJ, De-Wit MJ, Machacha T, Miller R (1995) Structural and tectonic controls of basin evolution in southwestern Gondwana during the Phanerozoic. In: Tankard AJ, Suárez SR, Welsink HJ (eds) Petroleum basins of South America. American Association of Petroleum Geologists, Memoir 62, pp 5–52

Thorpe RS, Francis PW, Harmon RS (1981) Andean andesites and crustal growth. Philos Trans R Soc Lond A 301:305–320

Veizer J, Buhl D, Diener A, Ebneth S, Podlaha OG, Bruckschen P, Jasper T, Korte Ch, Schaaf M, Ala D, Azmy K (1997) Strontium isotope stratigraphy: potential resolution and event correlation. Palaeogeogr Palaeoclimatol Palaeoecol 132:65–77

Vergara M, Nystrom JO, Cancino A (1995) Jurassic and early Cretaceous island arc volcanism, extension, and subsidence in the Coast Range of central Chile. Geol Soc Am Bull 107:1427–1440

Wigger PJ, Schmitz M, Araneda M, Asch G, Baldzuhn S, Giese P, Heinsohn WD, Martinez E, Ricaldi E, Röwer P, Viramonte J (1994) Variation in the crustal structure of the Southern Central Andes deduced from seismic refraction investigations. In: Reutter KJ, Scheuber E, Wigger PJ (eds) Tectonics of the Southern Central Andes. Springer, Berlin Heidelberg New York, pp 23–48

Wilson J, Dallmeyer RD, Grocott J (2000) New $^{40}Ar/^{39}Ar$ dates from the Las Tazas complex, northern Chile: Tectonic significance. J South Am Earth Sci 13:115–122

Wittmann S (2001) Wechselwirkungen zwischen karbonatischer und vulkaniklastischer Sedimentation auf dem jurassischen Vulkanbogen in der chilenisch/peruanischen Küstenkordillere (Südamerika), Doctoral Dissertation, Technical University of Berlin , School of Civil Engineering and Applied Geosciences, 2001–05-22 http://www.edocs.tu-berlin.de/diss/2001/wittmann_sonja.pdf (in German), 182p

Wörner G, Moorbath S, Horn S, Entenmann J, Harmon RS, Davidson JP, Lopez-Escobar L (1994) Large- and fine-scale variations along the Andean arc of northern Chile (17.5°–22°S). In: Reutter KJ, Scheuber E, Wigger PJ (eds) Tectonics of the Southern Central Andes, Springer, Berlin Heidelberg New York, pp 77–92